Composite Structures 267 (2021) 113917

Contents lists available at ScienceDirect

Composite Structures

journal homepage: www.elsevier.com/locate/compstruct

Data-driven machine learning approach for exploring and assessing mechanical properties of carbon nanotube-reinforced cement composites

J.S. Huang [a], J.X. Liew [b,1], K.M. Liew [a,*]

[a] Department of Architecture and Civil Engineering, City University of Hong Kong, Kowloon, Hong Kong, China
[b] Faculty of Applied Science, University of British Columbia, Kelowna, Bristish Columbia V1V 1V7, Canada

ARTICLE INFO

Keywords:
CNT-reinforced cement composites
Compressive and flexural strength
Predictive modeling
Mechanical attributes
Machine learning

ABSTRACT

Traditional experimental investigation on the mechanical properties of cement composites is deprecated due to the intensive time and labor involved. Existing predictive models can hardly map the complicated relationships among mechanical attributes and behavior. This study first adopts machine learning to predict the mechanical properties of carbon nanotube (CNT)-reinforced cement composites. For this purpose, predictive models are trained on the previously published experimental data and results demonstrate that machine learning models present better generalization ability and predictive performance than the traditional response surface methodology. A sensitivity analysis indicates that the factor having the maximum influence on compressive strength is the length of CNTs, whereas that having the maximum influence on flexural strength is the curing temperature. Thus, it can be concluded that compared with the traditional experimental investigation and regression methods, machine learning can efficiently and accurately predict the mechanical properties of CNT-reinforced cement composites.

1. Introduction

Cement-based composite materials, as the most widely used building materials in civil engineering structures, continuously attract substantial research attention. Developing high-performance and multifunctional cement composites has become a central issue in civil engineering [1]. To improve the strength and toughness of cement-based materials, their reinforcement from macroscale to nanoscale is required [2]. With the development of nanotechnology, nanomaterials are being increasingly used to reinforce cementitious materials [3]. Until now, the typical microfibers used to improve the performance of cementitious materials have included carbon fiber [4], polymeric fiber [5], glass fiber [6], steel fiber [7], and carbon nanotubes (CNTs) [8]. Among these, CNTs are the most extensively studied nanomaterials.

CNTs are the latest generation of fibers with length ranging from few nanometers to micrometers [9]. Due to their extraordinary mechanical properties, CNTs are considered a superior alternative to traditional fibers for the next generation of high-performance and multifunctional cement-based materials. CNTs can be typically classified into two types depending on the manufacturing process used: single-walled CNTs (SWCNTs) and multiwalled CNTs (MWCNTs) [10]. SWCNTs refer to a single layer of graphene rolled up into a cylindrical structure, whereas MWCNTs comprise multiple concentric SWCNTs bonded by interlayer van der Waals forces. The mechanism by which CNTs reinforce the cement matrix can be considered as a combination of four effects: bridging, filling, modifying, and nucleating [8]. The primary effect, bridging, depends on the ability of small-sized CNTs to form connections across nanometer-sized cracks, thus slowing the crack propagation and improving the strength [8,11].

Numerous experimental studies have investigated the mechanical properties of CNT-reinforced cement composites. Many factors affect the ultimate strength of composites and the CNT content is the most frequently studied factor. It has been reported that too few CNTs cannot connect across the microcracks, whereas too many CNTs will lead to cluster formation, and thus, reduce the reinforcing effect [12]. Luo et al. [13] studied the mechanical properties of silica fume-incorporated cement paste with 0.1, 0.5, and 1.0 wt% CNTs. The best improvements in flexural strength were obtained when 0.5 wt% CNTs were added. Sedaghatdoost and Behfarnia [14] investigated the mechanical strength of cement mortars containing 0.05, 0.1, and 0.15 wt% MWCNTs and found that the mortar incorporated with

* Corresponding author.
E-mail address: kmliew@cityu.edu.hk (K.M. Liew).
[1] This project was initiated by J.X. Liew.

https://doi.org/10.1016/j.compstruct.2021.113917
Received 23 December 2020; Accepted 24 March 2021
Available online 30 March 2021

0.1 wt% MWCNTs presented the highest increase in compressive, flexural, and tensile strength at the age of 28 and 90 days. In addition, the geometrical parameters of CNTs, such as diameter and length, substantially influence the mechanical properties of CNT-reinforced cement composites as the high aspect ratio (length to diameter) of CNTs enables them to form extensional contact with adjacent hydration products [15]. Al-Rub et al. [16] tested the flexural strength and ductility of cement paste containing different concentrations of long and short MWCNTs. They concluded that composites with low contents of long MWCNTs exhibit better mechanical performance than those with high contents of short MWCNTs. Konsta-Gdoutos et al. [2] examined the effect of MWCNTs' aspect ratio on the mechanical properties of cement paste. The results demonstrated that higher contents of short CNTs (aspect ratio: 700) were required to reach the same performance as that achieved by long CNTs (aspect ratio: 1600). In addition to the aforementioned influential parameters, other factors related to CNT treatment also play a role in the mechanical properties of cement composites reinforced by CNTs. For example, whether and how CNTs are functionalized substantially affect the mechanical strength of composites as the functional groups attached to the CNT surface play a role in the CNT-reinforcing mechanism [8]. Typical functional groups include carboxyl (–COOH) and hydroxyl (–OH) groups [17]. Li et al. [17,18] investigated the compressive and flexural strength of cementitious composites incorporating pristine and functionalized CNTs. It was clearly indicated that functionalized CNT-reinforced composites mechanically perform better than pristine CNT-reinforced composites. This conclusion was further verified by Chan and Andrawes [19], whose finite-element analysis revealed that CNT functionalization played a substantial role in improving the strength and ductility of cementitious composites. Finally, the homogeneous dispersion of CNTs is critical for preparing CNT-reinforced cementitious composites. Generally, the methods designed to disperse CNTs can be classified into physical and chemical methods. The physical methods provide external energy to avoid CNT agglomeration by breaking the van der Waals forces, such as sonication, ball milling, and mechanical stirring [20,21]. In contrast, chemical methods are introduced to add covalent or noncovalent bonds to improve the wettability of the CNT surface. In experimental research, these two methods are usually combined to obtain the best dispersion effect.

Besides the experimental investigation of the mechanical properties of CNT-reinforced cementitious materials, some studies have also focused on establishing a regression model between various influential factors and mechanical strength. Sobolkina et al. [22] proposed a regression model to map the relationships among the surfactant concentration, sonication time, and absorbance of an aqueous CNT dispersion. Using response surface methodology (RSM), Mohsen [15] investigated the effects of aspect ratio and CNT content on flexural and compressive strength. Similarly, Hassan et al. [23] used RSM to develop a model for predicting the compressive strength of mortar blocks. This model correlated the mechanical properties of mortar blocks with different influential parameters, such as wet and dry mixing of CNTs, sonication exposure time, whisking, and CNT concentration. Ramezani et al. [24] proposed analytical equations to predict the mechanical properties of CNT-reinforced cementitious materials. The influential parameters included CNT aspect ratio, concentration of CNT, ultrasonication procedure, water-to-cement (w/c) ratio, sand-to-cement (s/c) ratio, and testing age. Although the abovementioned studies have attempted to predict the mechanical strength of CNT-reinforced cementitious materials, they only considered mixture composition when constructing the model, while ignoring the influence of CNT properties and other parameters such as curing conditions. In addition, these methods usually consider the influencing factors individually and propose linear models that are not consistent with the complex underlying mechanism. Therefore, it is necessary to build models considering as many variables as possible and map the relationship realistically. The emergence of machine learning techniques enables the determination of the optimal mapping relationship between numerous factors and the mechanical strength of CNT-reinforced cementitious composites. Meanwhile, machine learning has already been used for predicting material properties. For instance, Rao and Mukherjee [25] presented a novel approach using an artificial neural network (ANN) to predict the micromechanical behaviors of ceramic matrix composites, and Reddy [26] proposed an ANN model to predict the strength properties of slurry-infiltrated fibrous concrete. Numerous studies have also focused on the use of ANN models in predicting the properties of composite materials [27,28]. In addition, support vector machine (SVMs) have also been successfully applied to construction-material problems, such as mixture design of concrete specimens [29–32].

The abovementioned traditional experimental investigations of the different factors influencing the mechanical properties of CNT-reinforced cement composites are mostly time-consuming and labor-intensive. Although some studies have attempted to predict the mechanical properties of composites according to a mixture design based on either a traditional regression model or an ANN model, these models have been developed through experimental design, which is significantly influenced by a priori knowledge of the experiment conductor, resulting in difficulty in exploring the true relationships. Moreover, the parameters investigated in previous studies were mostly mixture design, ignoring some other important influential factors. Additionally, few studies have used predictive models using the latest machine learning techniques for CNT-reinforced cement composites.

Motivated by these problems, this paper proposes a predictive model assisted by machine learning techniques, including ANN and SVM, to map the relationship between the mechanical properties of CNT-reinforced cement composites and multiple influential factors. The workflow of this study is illustrated in Fig. 1. Unlike previous studies on predicting mechanical strength based on an experimental design, the proposed model explores the relationships from previously published experimental results. This avoids the interference of a priori knowledge when designing experiments and ensures that the machine learning-assisted model can learn the true relationships between the mechanical properties of CNT-reinforced cement composites and the controlling parameters. A comprehensive investigation is performed on nine controlling parameters, covering not only the mixture composition but also the material properties and treatment conditions. This study supplements the application of machine learning techniques in the field of CNT-reinforced cement composites.

The rest of this paper is organized as follows. In Section 2, the abovementioned two machine learning techniques, ANN and SVM, are briefly introduced and some basic concepts are clarified. In Section 3, data acquisition and processing are introduced to obtain data for training and testing the network and different ANN structures, including the number of neurons and types of activation functions and optimizers, which are compared to identify the optimal ANN structure in this case. In addition, SVMs with different penalty coefficients and kernel functions are investigated, and their results are compared with those of ANNs and RSM analysis. Additionally, a sensitivity analysis is conducted on the input parameters to evaluate the relative importance of the input variables. In Section 4, the results and corresponding analysis are presented, and in Section 5, some conclusions and future prospects are presented.

2. Machine learning techniques

2.1. SVM

SVM, as a supervised learning method, can be widely applied to classification and regression analysis. The principal concept related to SVM lies in mapping the input data to a high-dimensional feature

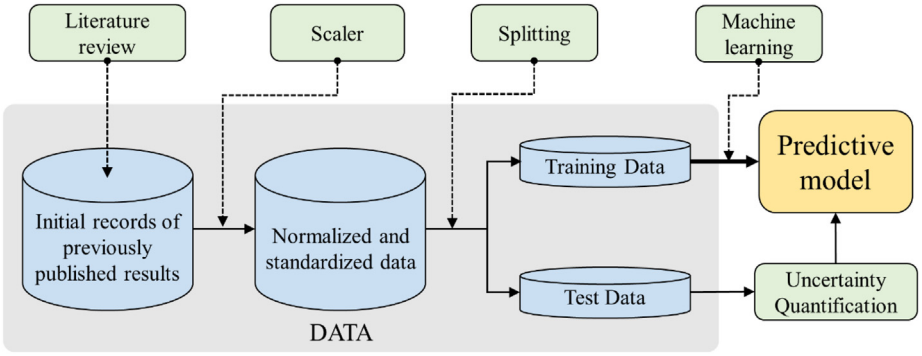

Fig. 1. Workflow of constructing a machine learning-assisted predictive model.

space, and subsequently, performing linear regression in the feature space [33]. Thus, the regression model for a SVM can be expressed as

$$f(x) = \sum_i^n \phi(x_i) w + b \tag{1}$$

where x_i is the input sample, w is a weight vector, b is the bias, and ϕ is a nonlinear mapping correlator. A standard SVM is designed to minimize two parameters: the norm of the squared weight vector, $\|w\|^2$, and the sum of allowable errors. These parameters are traded-off by a fixed penalty coefficient, C.

According to the SVM training methodology, there is no need to explicitly know the form of mapping correlator $\phi(x)$. Instead, only a kernel function, which maps the samples into a high-dimensional space, needs to be determined. The kernel function can be defined as a function that connects the dot products of the feature vectors to the vectors in the input space:

$$K(x, x_i) = \langle \phi(x_i), \phi(x) \rangle \tag{2}$$

By substituting the kernel function in the regression model, the entire problem can be solved in the input space itself:

$$f(x) = \sum_i^n (\beta_i - \beta_i^*) K(x_i) w + b \tag{3}$$

where β_i and β_i^* are two Lagrange multipliers related to minimizing the cost function. One of the most frequently used kernel functions is a Gaussian (or radial basis function, RBF) kernel, which can be expressed as

$$K(x_i, x_j) = exp\left\{ -\frac{\|x_i - x_j\|^2}{2\gamma^2} \right\} \tag{4}$$

where γ is a speed parameter to be optimized, which controls the generalization ability of an SVM. Other kernel functions include linear, poly, and sigmoid kernels.

2.2. ANNs

ANNs, which imitate the neural structure of the human brain, are known for their astonishing ability to automatically identify and extract key rules from raw input data. As one of the most popular and effective methods in machine learning, they have attracted considerable research interest [34,35]. A typical ANN system is composed of multiple layers, which contain multiple neurons, as shown in Fig. 2. A neuron is regarded as an individual calculation unit inside an ANN, and in each neuron, an activation function acts on its input and passes the result to its connected neurons, which can be represented as follows:

$$y_i = \sigma_i(W_i^k I_i + b_i) \tag{5}$$

where I_i denotes the input of neuron i, y_i denotes its output, σ_i is the activation function, W_i^k indicates the weight, and b_i is the bias. The common activation functions, presented in Table 1 and Fig. 3, include rectified linear unit (ReLU), sigmoid, tanh, exponential linear unit (ELU), and scaled exponential linear unit (SELU). An ANN usually comprises three or more layers, including one input layer, one output layer, and one or more hidden layers. The number of neurons in each layer varies considerably among different ANNs and cases.

Each connection between the neurons in an ANN corresponds to a weight parameter that indicates the strength of the connection. The goal of training an ANN is to learn the weights of the connections by minimizing a cost function over the training data:

$$L = \frac{1}{N} \sum_{n=1}^{N} \|y_r - y_o\|^2 \tag{6}$$

where L denotes the loss function, y_r is the real value, y_o is the output value, and N represents the number of training datasets. ANNs can be trained using different training algorithms, of which gradient descent using backpropagation is the most popular algorithm.

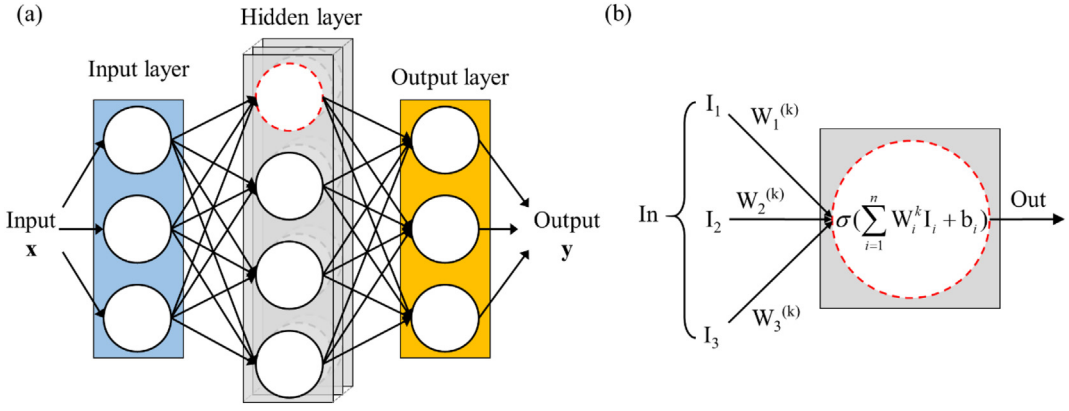

Fig. 2. A simple artificial neural network (ANN) and the computations performed by each neuron. (a) Generative ANN structure; (b) individual neurons in the hidden layer. (Modified after Ref. [36]).

Table 1
Different activation functions applied in an artificial neural network.

Activation function	Function formulation
Rectified linear unit	$\sigma(x) = \begin{cases} x & \text{if } x > 0 \\ 0 & \text{if } x \le 0 \end{cases}$
Sigmoid	$\sigma(x) = \frac{1}{1+exp(-x)}$
Tanh	$\sigma(x) = 2\text{Sigmoid}(2x) - 1$
Softplus	$\sigma(x) = ln(1 + e^x)$
Scaled exponential linear unit	$\sigma(x) = \lambda \begin{cases} x & \text{if } x > 0 \\ \alpha exp(x) - \alpha & \text{if } x \le 0 \end{cases}$

Note: α is a positive adjustable parameter, which controls the negative part of the exponential linear unit function, and λ is a parameter >1.

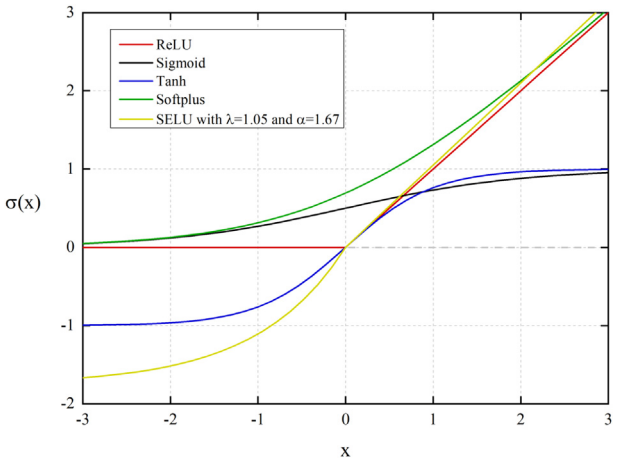

Fig. 3. Commonly used activation functions in an artificial neural network: Sigmoid, rectified linear unit (ReLU), Tanh, Softplus, scaled exponential linear unit (SELU).

3. Data and methods

3.1. Data acquisition and preprocessing

To develop an ANN model, a comprehensive dataset that can cover various parameters affecting the mechanical behavior of CNT-reinforced cementitious composites is required. In this study, the required dataset is established through a literature search and contains 114 experimental samples, whose features are presented in Table 2. The raw sample data can be accessed from Table A1 in the Appendix. Among these, samples 1–2 are acquired from [17], samples 3–26 from [37], samples 27–30 from [38], samples 31–36 from [39], samples 37–38 from [18], samples 39–86 from [15], samples 87–96 from [40], samples 97–107 from [41], and samples 108–114 from [42]. These 114 samples are further classified into training and testing samples based on a training–testing split rate of 0.2.

An important step to be followed before ANN training is to preprocess the input and output data. Preprocessing transforms the raw data into a form more suitable for network use. In this case, the preprocessing is mainly performed on two parameters, the external diameter and length of CNTs. As the raw data provided in the original work are in the form of a value range, which is unsuitable for network use, the mean value of the upper and lower limits is adopted for these two parameters.

Another important procedure influencing the effectiveness of an ANN is the normalization of raw data. Data normalization is a mathematical method used to scale the input and output variables in the same range of values, which can minimize biases within the neural network for one parameter to another. By conducting data normalization, the training of ANN can be accelerated. Various data normalization methods are available. In this case, MinMaxScaler and StandardScaler are adopted for ANNs and SVMs, respectively, and their principles are illustrated in Eqs. (7) and (8), respectively.

$$X_{MMscaled} = \frac{X - X_{min}}{X_{max} - X_{min}}(max - min) + min \tag{7}$$

where $X_{MMscaled}$ represents the value obtained after MinMaxScaling; X_{max} and X_{min} refer to the maximum and minimum values for a specific parameter; and *max* and *min* are the upper and lower limits of the range obtained after scaling. In this case, $max = 1$ and $min = 0$ are considered.

$$X_{Sscaled} = \frac{X - X_{mean}}{s} \tag{8}$$

where $X_{Sscaled}$ is the value obtained after StandardScaling, X_{mean} is the mean of the training samples, and s is their standard deviation.

3.2. ANN model

The structure of an ANN model depends on the number of layers in a network, the number of neurons in each layer, and the activation function at each layer. The optimal structure of an ANN highly

Table 2
Feature descriptions of training and testing data collected from the literature.

Variables	Minimum value	Maximum value	Mean value	Description
Input variables				
Type of cement	1	2	–	I_1, discontinuous value (1 and 2)
Water-to-cement ratio	0.200	0.500	0.367	I_2, continuous value
Content of carbon nanotubes	0.000	0.008	0.002	I_3, continuous value
External diameter (nm)	4.000	250.250	19.974	I_4, continuous value
Length (μm)	1.000	250.250	21.588	I_5, continuous value
Functionalization method	1	4	–	I_6, discontinuous value (1, 2, 3 and 4)
Curing days	3.000	28.000	20.623	I_7, continuous value
Curing temperature (°C)	20.000	30.000	23.193	I_8, continuous value
Dispersion method	1	5	–	I_9, discontinuous value (1, 2, 3, 4, and 5)
Output variables				
CS (MPa)	27.300	154.400	73.132	O_1, continuous value
FS (MPa)	4.000	16.900	10.255	O_2, continuous value

Notes: For type of cement, 1 indicates ordinary Portland cement, Cement I, Class 42.5 R and 2 indicates Portland cement, Cement I, Class 52.5 R.
For functionalization method, 1 indicates no functionalization, 2 indicates functionalization in carboxyl solution, 3 indicates functionalization in hydroxyl solution, and 4 indicates functionalization in other acid solution.
For dispersion method, 1 indicates no dispersion, 2 indicates sonicated in polycarboxylate solution, 3 indicates sonicated in TNWDIS (an aromatic modified polyethylene glycol ether), 4 indicates sonicated in gum arabic, and 5 indicates sonicated in water.
For compressive and flexural strength, all data are rounded off to the nearest tenth to make the data uniform.

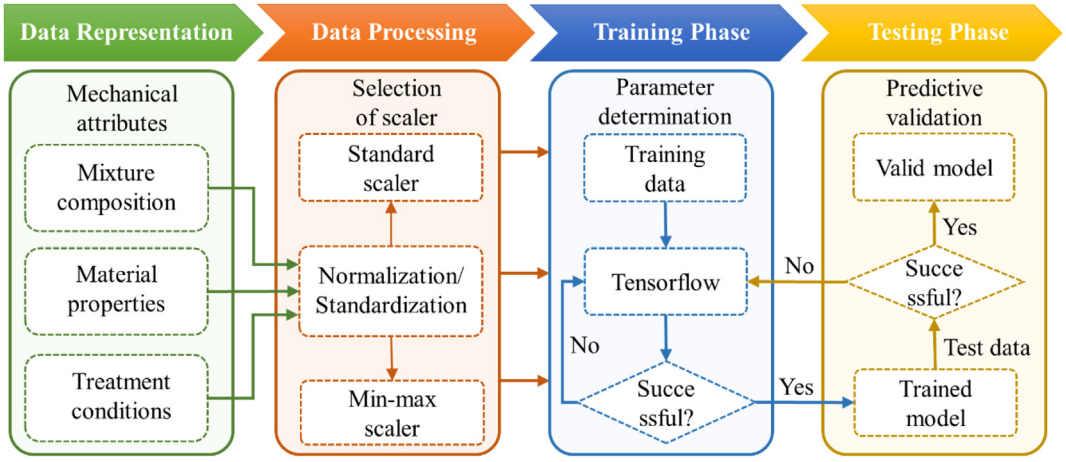

Fig. 4. Methodology of ANN development.

Table 3
Artificial neural network parameters: carbon nanotube-reinforced cement composite strength prediction problem.

Parameters	Description
Number of neurons in the input layer	9
Number of neurons in the output layer	2
Number of hidden layers	1–3
Number of neurons in the hidden layers	10–90
Activation functions for hidden layers	ReLU, Sigmoid, Softplus, SELU, Tanh
Activation function for output layer	Linear
Number of samples in dataset	114
Optimizer	Adam, Adagrad, Adadelta, RMSprop
Training–testing split	0.2

depends on the problem represented by the network. ANN performance is evaluated by considering two parameters: coefficient of determination (R^2) (Eq. (9)) and mean squared error (MSE) (Eq. (10)).

$$R^2 = 1 - \frac{\sum_{i=1}^{N}(t_i - a_i)^2}{\sum_{i=1}^{N}(t_i - t_{ia})^2} \tag{9}$$

$$MSE = \frac{1}{N}\sum_{i=1}^{N}(t_i - a_i)^2 \tag{10}$$

where N represents the number of samples, t_i indicates the target output, a_i is the network output, and t_{ia} indicates the average of the target output.

In this study, an ANN analysis is performed using Tensorflow. ANNs with 3–5 layers are investigated and different numbers of neurons contained in the hidden layer are also used to determine the optimal ANN structure. Multilayered feedforward networks trained with back Levenerg–Marquardt propagation have been used in the strength prediction model. The training process is terminated at the point where the validation loss no longer decreases. Fig. 4 shows the methodology of ANN development. The detailed network configuration and the parameters used for predicting the mechanical properties are shown in Table 3.

After selecting the network structure, the ANN is trained to map the relationship between the input variables and the corresponding output variables. In this process, 91 samples are used. After determining the optimal ANN structure, different optimizers and activation functions are adopted to evaluate their influences on the final output. The remaining 23 samples not used in network training are used for network testing once the training is complete. The testing is performed using the ANN model with optimal structures. The ANN then predicts the compressive and flexural strength for these samples. The values predicted by the ANN are compared with the experimental values to evaluate the performance of the ANN. Additionally, the dataset itself is duplicated to investigate the influence of the number of training samples on the performance of the ANN model.

3.3. SVM

Two SVMs are used to map the relationship between nine input variables and two output variables. The parameter settings for these two SVMs are identical, as shown in Table 4. Different penalty coefficients and kernel functions are investigated together to determine the optimal SVM for this problem. After the optimal SVM is chosen, the dataset itself will be duplicated to investigate the effect of the number of training samples on the performance of SVM.

3.4. RSM

The influence of the nine input variables on the compressive strength (CS) and flexural strength (FS) is investigated using traditional regression methods, such as RSM. Using the JMP software, the central composite design method is adopted to determine the desirability function between the final output and study variables. The following methodology is used to perform this analysis.

(1) The factors are modeled by fitting a second-order polynomial equation model. Second-order polynomial equations are applied to represent the CS and FS as functions of independent variables. Herein, the three variables with discontinuous values (I_1, I_6, and I_9) are not considered.

Table 4
Support vector machine parameters: carbon nanotube-reinforced cement composite strength prediction problem.

Parameters	Description
Number of support vector machines	2
Number of input variables	9
Number of output variable	1
Normalization scaler on input data	StandardScaler
Penalty coefficient, C	1, 5 ,10, 20, 50, 100
Kernel functions	Radial basis function, Linear, Poly (degree = 2), Sigmoid
Training–testing split	0.2

$$O_1 = a_0 + \sum_i a_i I_i + \sum_i a_{ii} I_i^2 + \sum_{i,j,i<j} a_{ij} I_i I_j \quad i,j = 2,3,4,5,7,8 \tag{11}$$

$$O_2 = b_0 + \sum_i b_i I_i + \sum_i b_{ii} I_i^2 + \sum_{i,j,i<j} b_{ij} I_i I_j \quad i,j = 2,3,4,5,7,8 \tag{12}$$

where a_i and b_i are the response surface coefficients.

(2) The response surface coefficients are determined using a central composite design type with six center points.
(3) The R^2 and MSE values of the prediction models are recorded.

3.5. Sensitivity analysis

In this study, the Jacobian matrix is used to analyze the attribution weights of different parameters influencing the output strength. A larger absolute value of the weight coefficient indicates a more significant influence on the final output. The positive and negative symbols usually refer to the positive and negative correlations between the input parameters and output values, respectively.

4. Results and discussion

4.1. Neural networks with one hidden layer

Fig. 5 shows the training and testing processes for ANNs with one hidden layer. Here, the training loss continuously decreases with an increase in the number of epochs, whereas the testing loss first decreases and then increases. The contrasting trends of the two losses can be explained as follows. The training loss decreases as the network parameter keeps updating and the mapping relationship in the training data becomes increasingly precise. However, for the testing data, as the training process proceeds, the model becomes increasingly complicated. The updated parameters suitable for the training samples are likely to be unsuitable for the testing samples. This generates a turning point in the testing loss curve, which divides the entire process into the overfit zone and other zones. The underfit zone is the area where the testing loss is too large (MSE > 100). The epoch corresponding to the turning point is usually the epoch best fitted to a specific ANN model,

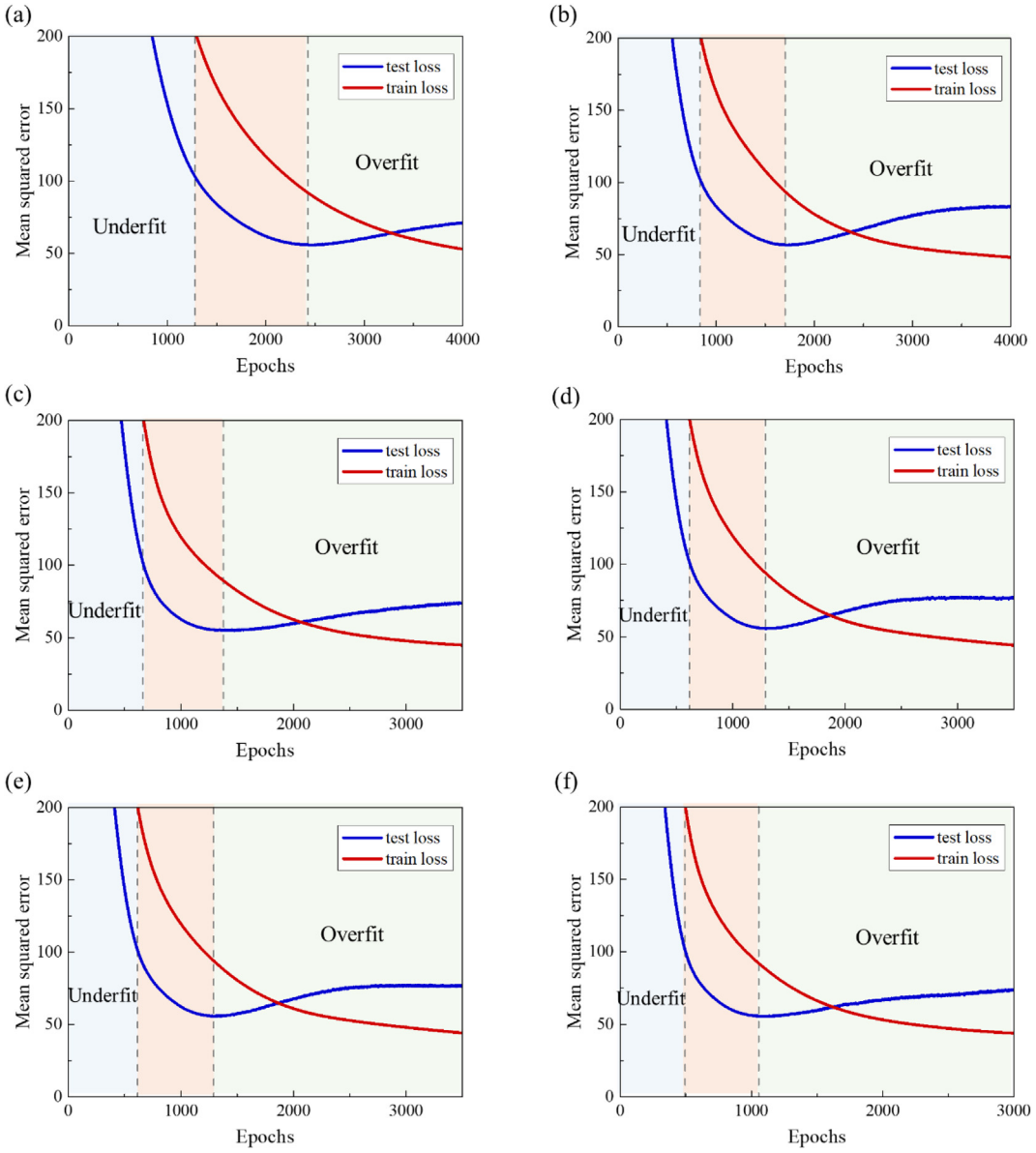

Fig. 5. Training and testing losses for artificial neural networks (ANNs) with one hidden layer. The rectified linear unit activation function and Adam optimizer are adopted for these ANNs: (a) 9–10-2, (b) 9–20-2, (c) 9–30-2, (d) 9–40-2, (e) 9–50-2, and (f) 9–60-2.

Table 5
Mean squared error and R^2 values for training and testing sets of artificial neural networks with one hidden layer. Each value is an average of 10 simulations.

Neurons in each layer	Trainable parameters	Training sets		Testing sets		Turning point
		MSE	R^2	MSE	R^2	
9–10-2	122	94.890	0.770	55.882	0.848	2300–2600
9–20-2	242	93.141	0.785	55.838	0.848	1600–1800
9–30-2	362	92.592	0.787	56.586	0.846	1400–1500
9–40-2	482	89.574	0.796	55.762	0.848	1300–1400
9–50-2	602	91.761	0.791	55.764	0.848	1100–1200
9–60-2	722	93.850	0.776	55.835	0.848	950–1050

which is also the point where the best performance of the model can be obtained. Table 5 presents the detailed information about the training and testing processes of ANNs with one hidden layer. Evidently, the turning point moves to earlier epochs with an increase in the number of neurons in the hidden layer, which means that a faster training process can be obtained by increasing the number of neurons in the hidden layer. The MSE and R^2 values for the testing sets are identical for ANNs with different numbers of neurons in the hidden layer, whereas the training MSE values are the minimum and training R^2 values are the maximum for the case of 9-40-2, as clearly observed in Fig. 6. This trend is related to the corresponding network size.

4.2. Multilayer enhanced neural networks

Section 4.1 illustrates the performance of different neural networks with one hidden layer. As observed from the previous results, a further improvement on the training and testing performances can be made by increasing the network depth. An ANN with more layers usually presents a stronger ability to handle complicated decisions and multiple interactions among parameters. In this section, several ANNs containing two or three hidden layers are investigated, and the training and testing losses are presented in Figs. 7 and 8, respectively. In these figures, the moving trend of the turning point is similar to that of ANNs with one hidden layer. As the network depth increases, the turning point emerges earlier, leading to a faster convergence speed. However, as shown in Table 6, an increase in the number of hidden layers does not improve the ANN performance in reducing the training and testing losses. Combining the results of ANNs with one hidden layer, the performance of these networks is strongly associated with the number of trainable parameters, which is optimally ~ 500. If the number of trainable parameters is less than the optimal value, there will be too few parameters to explore the information contained in the input variables. In contrast, if the number is too large, neurons will be wasted and redundant information will be transferred, resulting in additional loss. Thus, it is important to focus on the number of trainable parameters to determine the optimal structure of an ANN.

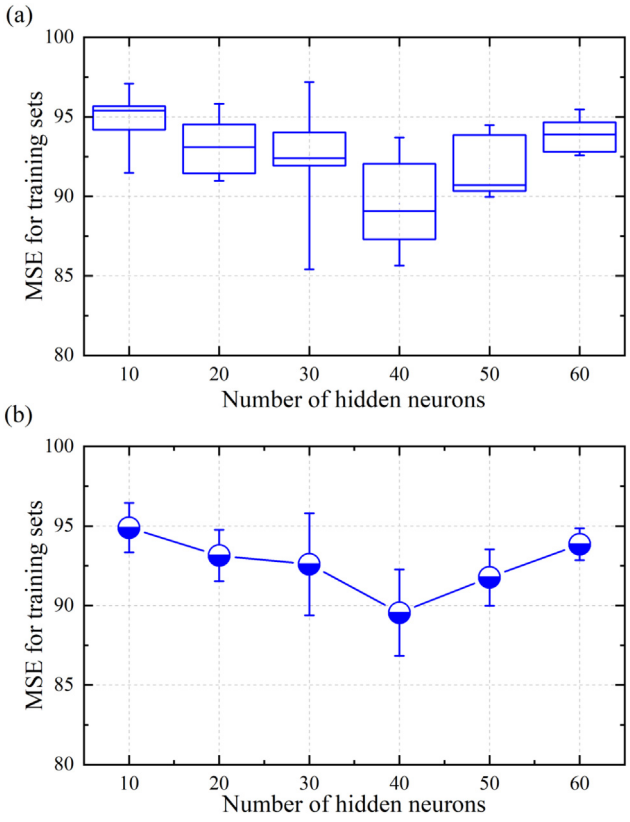

Fig. 6. (a) Box–whiskers plot of training mean squared error with different numbers of hidden neurons. (b) Mean plus or minus one standard deviation. Each value is a mean of 10 simulations. The rectified linear unit activation function and Adam optimizer are used for these artificial neural networks.

4.3. Optimal ANN structure

As suggested in the previous section, the ANN performance is strongly related to the number of trainable parameters. The aforementioned results indicate that the optimal number of trainable parameters is ~ 500. Therefore, several ANNs with ~ 500 trainable parameters are investigated and the corresponding results are presented in Table 7. The table clearly shows that the structure of 9–17-17–2 (Fig. 9) with 512 trainable parameters exhibits the best performance in terms of both MSE and R^2 for the training and testing sets. In the next section, this structure will be applied to all ANNs to investigate other properties.

4.4. Activation function and optimization algorithm

So far, the ReLU activation function has been used to map the input and output for the previous network. An appropriate activation function is important as it affects the formatting of the input data. The 9–17-17–2 network is trained with different activation functions in the hidden layer and the corresponding results are shown in Fig. 10, where the Tanh function is observed to exhibit the best performance in training loss but a very slow convergence speed. The SELU function exhibits high performance in both training and testing losses. In addition, SELU presents a relatively fast convergency speed. Overall, SELU performs best among the five most frequently used activation functions.

In addition to the activation function, the choice of optimizer is also key to obtain suitable performance for a given ANN. A comparison among different optimizers is illustrated in Fig. 11, where the activation function in the hidden layer is selected as the SELU function. The results indicate that the Adadelta optimizer exhibits the best performance in terms of both loss and convergence speed. Other optimizers do not show competitive advantages over Adadelta in this problem.

Table 8 shows the results for the training and testing sets with 9–17-17–2 architecture at the turning point. These results indicate that

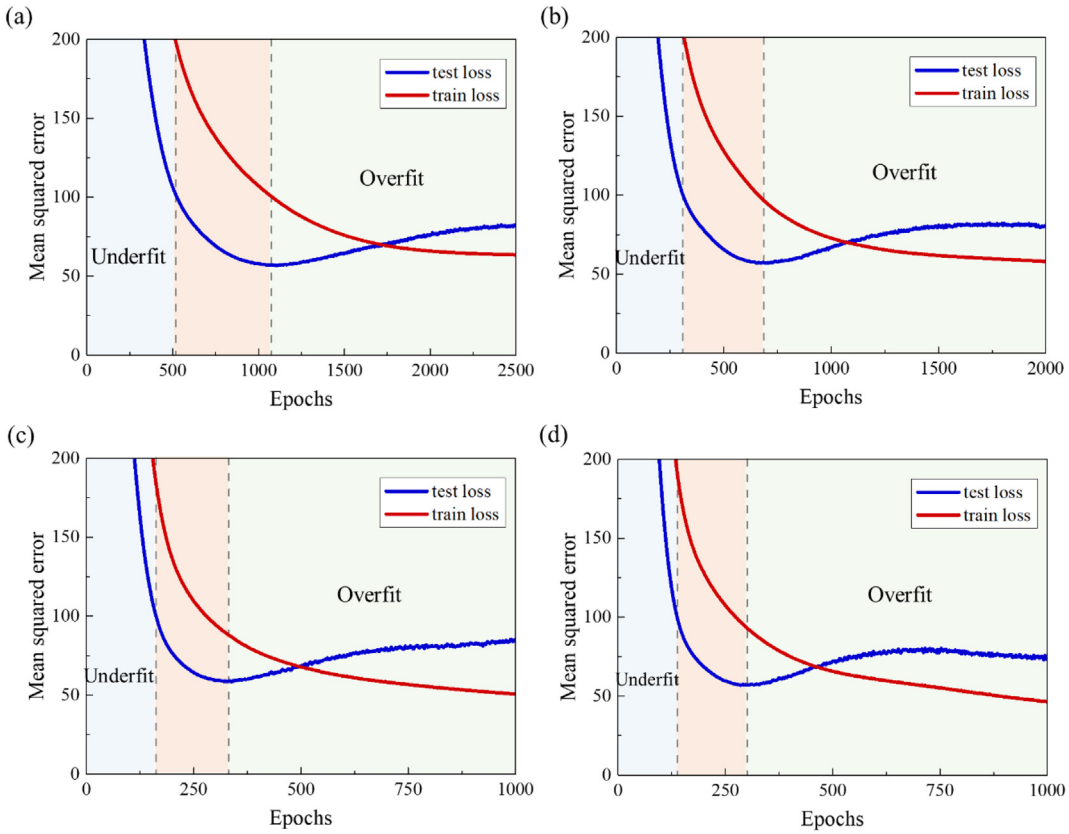

Fig. 7. Training and testing losses for artificial neural networks (ANNs) with two hidden layers. The rectified linear unit activation function and Adam optimizer are adopted for these ANNs: (a) 9–10-10–2, (b) 9–20-20–2, (c) 9–30-30–2, and (d) 9–40-40–2.

the highest R^2 value for the training set is achieved when the combination of the Adadelta optimizer and Sigmoid function is used. However, the highest R^2 value for the testing set is achieved using the Adadelta optimizer and Tanh function. As the generalization ability of an ANN is more important than the memorizing ability, the combination achieving the highest R^2 value for the testing set is considered the optimal combination, i.e., Adadelta and Tanh. The training and testing processes of 9–17-17–2 with the Adadelta optimizer and Tanh function are shown in Fig. 12.

4.5. Network testing

For network testing, the 23 remaining samples are used on the trained network. The testing results of network 9–17-17–2 obtained with the Tanh activation function and Adadelta optimizer are presented in Fig. 13. As shown, the values predicted by the ANN model for the remaining datasets match well with the experimental values. The occasional inconsistency between the predicted and experimental values can be mainly attributed to the fact that there are many undefined parameters in this model, which undoubtedly influences the accuracy of the ANN model. Hence, the results indicate that the ANN model can be applied to the strength prediction of CNT-reinforced cementitious composites. However, to obtain better accuracy, it is recommended to reduce the number of undefined influential parameters as much as possible in the future.

4.6. SVMs

The prediction results obtained using SVM techniques are presented in Table 9. The results demonstrate that in this problem, the RBF kernel presents the best performance among these commonly used kernels. Moreover, as the value of the penalty coefficient increases, the values of both R^2 and MSE also increase. The results suggest that the minimum MSE can be achieved using the RBF kernel and a penalty coefficient of 20. The SVM does not perform as well as the ANN model (R^2 = 0.908), as the MSE obtained for the testing sets in the ANN was much smaller than that in the SVM. Thus, ANN outperforms SVM in this problem.

4.7. Influence of size of training datasets

The number of training samples is a key factor influencing the performance of the machine learning techniques. Generally, more training samples ensure that the learner can fully understand and study the inner pattern of the data, resulting in a more accurate prediction. Herein, the training sets are augmented by duplicating the training sets themselves. The duplication factor is set as 1, 2, 5, 10, 50, and 100. The influence of the duplication coefficient on the MSE and R^2 of the testing sets for both ANN and SVM is presented in Table 10. The results show that the increase in the number of training samples has a significant positive influence on SVM performance. With more training samples provided, the SVM can completely mine the knowledge behind the data and perform more precise prediction. However, this is not the case for ANNs, as increasing training samples have little effect on ANN performance. The ANN outperforms the SVM for small datasets, whereas the SVM performs better on large datasets. Moreover, the ANN can explain and understand the data pattern with only a few training samples, whereas more training samples are required for the SVM to fully understand the pattern.

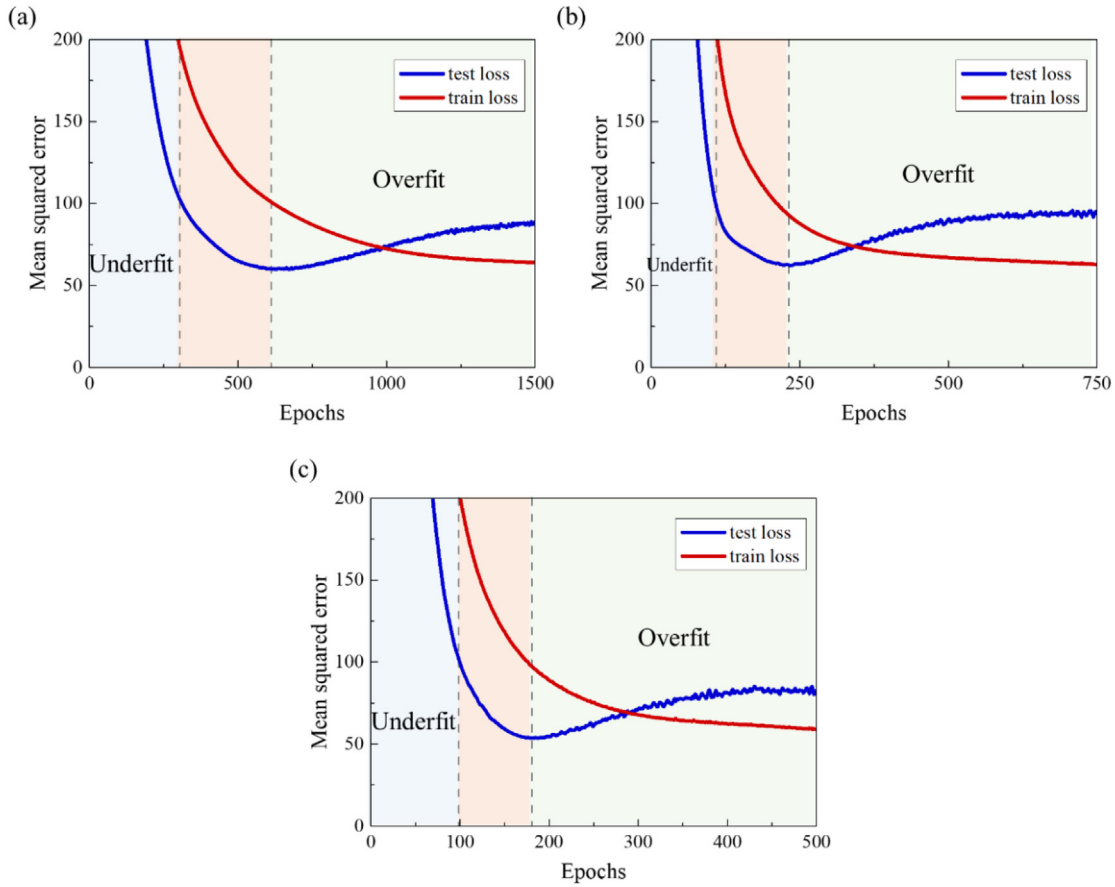

Fig. 8. Training and testing losses for artificial neural networks (ANNs) with two hidden layers. The rectified linear unit activation function and Adam optimizer are adopted for these ANNs: (a) 9-10-10-10-2, (b) 9-20-20-20-2, and (c) 9-30-30-30-2.

Table 6
Mean squared error and R^2 values for training and testing sets of artificial neural networks (ANNs) with two and three hidden layers. The rectified linear unit activation function and Adam optimizer are adopted for these ANNs. Each value is an average of 10 simulations.

Neurons at each layer	Trainable parameters	Training sets		Testing sets		Turning points
		MSE	R^2	MSE	R^2	
9–10-10–2	232	93.270	0.776	56.905	0.845	1000–1100
9–20-20–2	662	92.136	0.784	56.628	0.846	450–400
9–30-30–2	1292	94.172	0.777	57.211	0.844	350–400
9–40-40–2	2122	94.368	0.783	56.850	0.845	300–350
9–10–10–10-2	342	92.883	0.770	57.556	0.843	550–650
9–20–20–20-2	1082	93.924	0.785	59.269	0.839	200–250
9–30–30–30-2	2222	92.839	0.783	59.217	0.839	150–200

Table 7
Mean squared error and R^2 values for training and testing sets of artificial neural networks (ANNs) with two and three hidden layers. The rectified linear unit activation function and Adam optimizer are adopted for these ANNs. Each value is an average of 10 simulations.

Neurons at each layer	Trainable parameters	Training sets		Testing sets	
		MSE	R^2	MSE	R^2
9–15-15–2	422	90.567	0.775	56.740	0.846
9–16-16–2	466	90.159	0.799	57.348	0.844
9–17-17–2	512	89.314	0.801	56.123	0.846
9–18-18–2	560	90.833	0.783	56.631	0.846
9–11–11–11-2	398	91.953	0.783	57.402	0.844
9–12–12–12-2	458	90.365	0.784	58.090	0.842
9–13–13–13-2	522	89.556	0.792	60.396	0.836

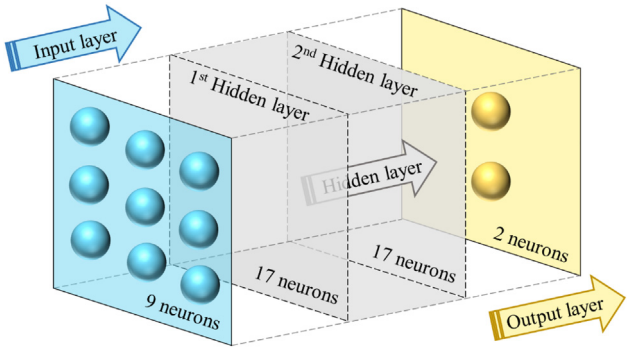

Fig. 9. Structure of artificial neural network model with optimal predictive performance.

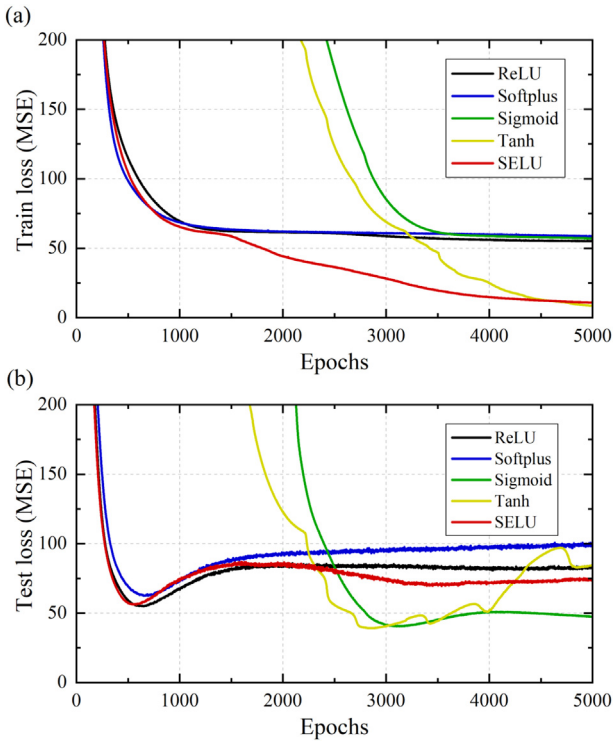

Fig. 10. Mean squared error of (a) training sets and (b) testing sets for 9–17-17–2 network: comparisons among various activation functions. The Adam optimizer is used for these ANNs.

4.8. RSM analysis

The RSM analysis results presented in Table 11 indicate that the R^2 values for both compressive strength (-4.91) and flexural strength (-0.86) are negative, which suggests that RSM is far from capable of revealing the intricate true relationship. Compared with the ANN and SVM (Fig. 14), the predictive values for both compressive strength and flexural strength diverge from the experimental values in the RSM model, representing a weaker generalization ability for new data. Traditional RSMs are simpler but cannot completely understand the pattern hidden in the data, and will gradually be replaced by newly emerging machine learning techniques in future applications.

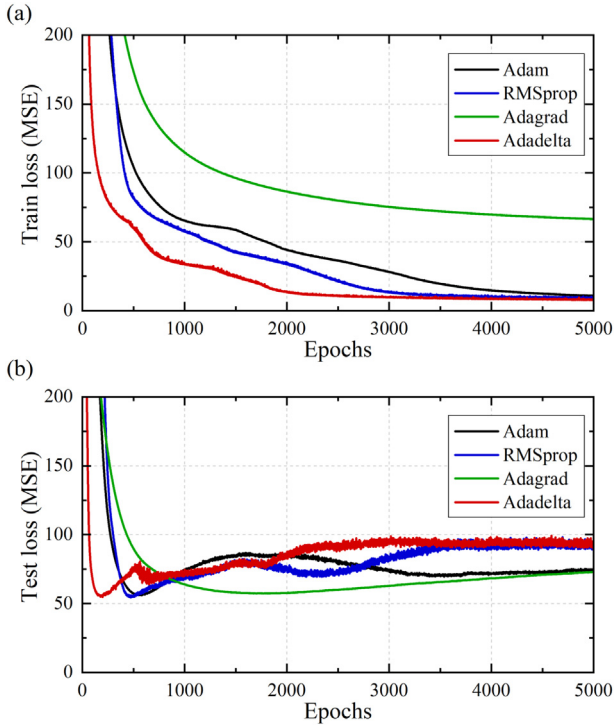

Fig. 11. Mean squared error of (a) training sets and (b) testing sets for 9–17-17–2 network: comparisons among various optimizers. The SELU activation function is adopted for these ANNs.

4.9. Sensitivity analysis

The evaluated Jacobian matrix is presented in Table 12. The computation results demonstrate that the CNT length is the most influential factor for compressive strength, and the curing temperature is the most influential factor for flexural strength. The significance of the sensitivity analysis lies in the consideration of the principal influential parameters when designing CNT-reinforced cementitious composites.

5. Conclusions

In this study, machine learning techniques, including ANNs and SVMs, are developed for predicting the compressive and flexural strengths of CNT-reinforced cementitious composites. The ANNs and SVMs are trained with 91 samples and tested with 23 samples acquired from the literature. The following conclusions can be drawn.

(1) Both ANNs and SVMs are suitable for predicting the mechanical properties of CNT-reinforced cementitious composites and outperform traditional RMS analysis. The 9–17-17–2 network with the activation function Tanh and optimizer Adadelta exhibits the best performance for ANN training, and SVMs with the RBF kernel and penalty coefficient of 20 outperform other SVMs. Comparisons between ANNs and SVMs show that ANNs perform better on small datasets, whereas SVMs are more suitable for large datasets.
(2) Prediction of the strength properties of CNT-reinforced cementitious composites does not present a perfect match with the experimental data, which is mainly attributed to the existence

Table 8
The R^2 values obtained for the training and testing sets of ANNs with 9–17-17–2 architecture at the turning points: comparisons among various optimizers and activation functions. Each value is an average of 10 simulations.

Optimizer	Adam		Adagrad		Adadelta		RMSprop	
Activation function	Train	Test	Train	Test	Train	Test	Train	Test
SELU	0.803	0.847	0.789	0.849	0.803	0.851	0.795	0.851
ReLU	0.801	0.842	0.784	0.846	0.796	0.851	0.794	0.848
Sigmoid	−0.130	−0.002	0.836	0.888	0.843	0.886	−0.117	−0.002
Softplus	0.818	0.826	0.814	0.830	0.801	0.847	0.805	0.836
Tanh	0.835	0.907	0.807	0.894	0.838	0.908	−0.126	−0.002

Notes: negative values indicate that the network converges to a local optimum instead of the global optimum.

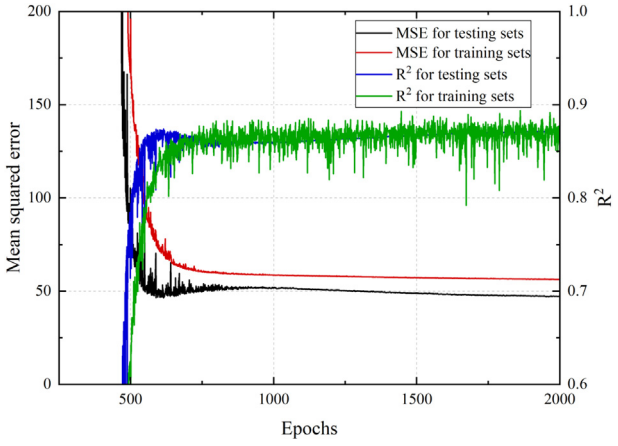

Fig. 12. Training and testing progress of the 9–17-17–2 network with Tanh activation function and Adadelta optimizer.

of undefined influential parameters. This is uncontrollable when attaining data from previously published articles, as there are many factors that are not clearly mentioned and clarified in the literature.

(3) The sensitivity analysis results show that the CNT length is the most influential parameter for compressive strength, whereas the curing temperature is the most influential factor for flexural strength, which provides information to optimize the mixture and condition design for future experiments on CNT-reinforced cement composites.

Due to the limitation of the data resources, there are still several inadequacies related to this model. Several parameters that control the mechanical properties of CNT-reinforced cementitious composites are still absent from this model, such as the properties of additives, sonication time and energy, and curing humidity. Besides, the literature data contain many undefined factors influencing the accuracy of

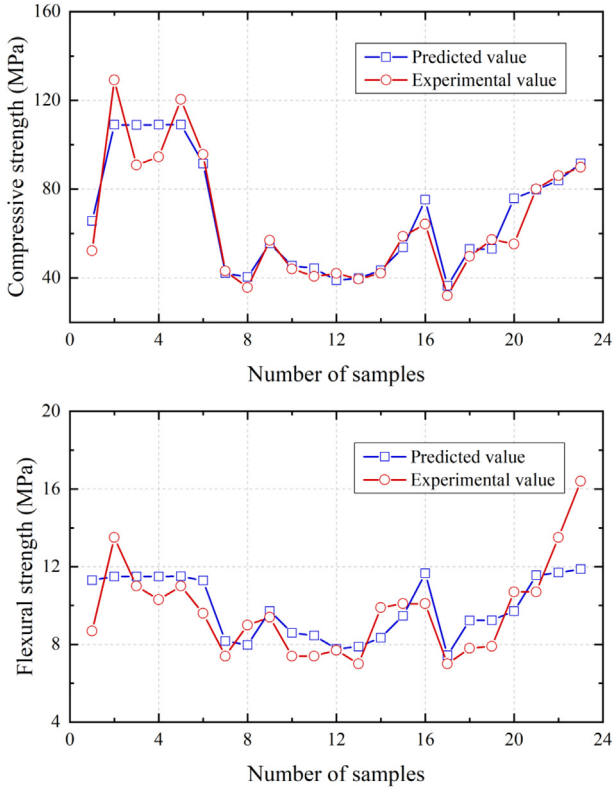

Fig. 13. Testing results for 9–17-17–2 network with Tanh activation function and Adadelta optimizer.

Table 9
R^2 and mean squared error values for testing sets of SVMs: comparisons among various kernels and penalty coefficients. Each value is an average of 10 simulations.

Kernel	RBF		Linear		Poly (degree = 2)		Sigmoid	
Penalty coefficient	R^2	MSE	R^2	MSE	R^2	MSE	R^2	MSE
1	0.804	342.083	0.847	190.852	0.765	351.102	0.814	271.751
5	0.853	160.296	0.852	184.183	0.820	308.110	0.826	221.992
10	0.879	153.188	0.859	179.174	0.856	221.163	0.842	170.524
20	0.900	121.077	0.866	145.264	0.868	205.690	0.861	154.675
50	0.902	132.605	0.869	152.637	0.847	210.761	0.869	165.180
100	0.902	135.844	0.875	159.115	0.861	207.174	0.871	168.805

Table 10
Mean squared error and R^2 values of testing sets for both ANN (9–17-17–2 with Adadelta optimizer and Tanh function) and SVM (C = 20 and RBF kernel): influence of duplication factor.

Models	ANN		SVM	
Duplication factor	MSE	R^2	MSE	R^2
1	33.835	0.908	121.077	0.900
2	39.8794	0.908	163.491	0.920
5	35.463	0.908	36.483	0.966
10	34.314	0.908	41.379	0.971
50	34.236	0.905	21.050	0.985
100	34.428	0.904	32.999	0.988

Table 11
Results of response surface methodology analysis.

Output	MSE	R^2
Compressive strength	5159.8	−4.91
Flexural strength	92.1	−0.86

the machine learning model. For example, the testing methods and procedures cannot be the same for all experiments; this factor is ignored in the current model. The difference among these undefined parameters will undoubtedly affect the final output, which is not and cannot be considered at this stage. These limitations are the main sources that degrade the accuracy of machine learning models.

Extended studies are required to incorporate more influential factors into the model to predict the mechanical properties of CNT-reinforced cementitious materials. The greater is the number of parameters considered in the model, the lesser is the impact that the undefined parameters will have on the final output. To achieve this, machine learning-assisted prediction combined with an experimental design is a promising option.

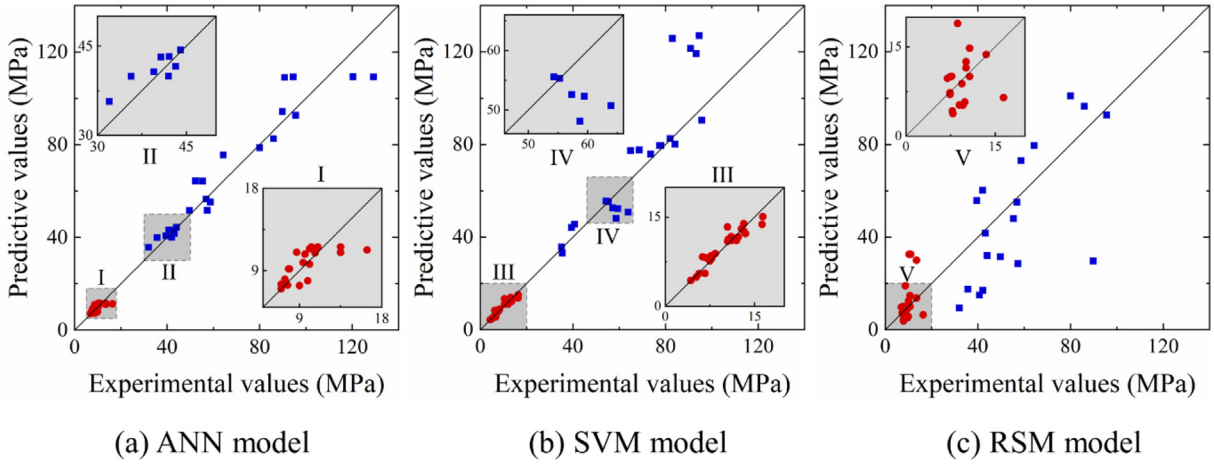

Fig. 14. Comparison among machine learning models and response surface methodology model. Red circles indicate flexural strength and blue squares indicate compressive strength.

Table 12
Jacobian weight coefficient matrix for input variables.

Variables	Weight coefficient			
	Compressive strength	Ranking	Flexural strength	Ranking
Type of cement	0.1570	3	−0.0031	9
Water-to-cement ratio	−0.0215	7	−0.0070	8
Contents of CNTs	−0.0136	8	0.0328	7
External diameter	0.0306	6	−0.2043	3
Length	−0.2171	**1**	−0.2980	2
Functionalization method	−0.2020	2	−0.1056	5
Curing days	0.0512	4	0.0809	6
Curing temperature	0.0435	5	0.3031	**1**
Dispersion method	−0.0129	9	−0.1226	4

Table A1
Raw input and output data obtained from previously published literatures.

Input										Output	
No	Composites composition			Properties of CNTs			Treatment conditions			Mechanical properties	
	Type of cement	w/c	Content of CNTs	External diameter (nm)	Length (μm)	Functionalization method	Curing days	Curing temperature (℃)	Dispersion method	CS (MPa)	FS (MPa)
1	1	0.45	0.000%	10–30	0.5–500	2	28	30	1	52.3	6.7
2	1	0.45	0.500%	10–30	0.5–500	2	28	30	1	62.1	8.4
3	1	0.2	0.100%	0–8	0.5–2	1	28	20	2	101.2	9.1
4	1	0.2	0.500%	0–8	0.5–2	1	28	20	2	116.9	10.6
5	1	0.2	0.800%	0–8	0.5–2	1	28	20	2	74.1	9.0
6	1	0.2	0.100%	20–30	0.5–2	1	28	20	2	129.2	13.5
7	1	0.2	0.500%	20–30	0.5–2	1	28	20	2	136.4	11.1
8	1	0.2	0.800%	20–30	0.5–2	1	28	20	2	138.1	11.9
9	1	0.2	0.100%	0–8	10–30	1	28	20	2	116.2	12.9
10	1	0.2	0.500%	0–8	10–30	1	28	20	2	107.6	11.9
11	1	0.2	0.800%	0–8	10–30	1	28	20	2	113.2	12.4
12	1	0.2	0.100%	20–30	10–30	1	28	20	2	124.6	12.6
13	1	0.2	0.500%	20–30	10–30	1	28	20	2	110.7	12.0
14	1	0.2	0.800%	20–30	10–30	1	28	20	2	121.9	12.6
15	1	0.2	0.100%	0–8	0.5–2	3	28	20	2	90.8	11.0
16	1	0.2	0.500%	0–8	0.5–2	3	28	20	2	152.1	15.3
17	1	0.2	0.800%	0–8	0.5–2	3	28	20	2	93.2	7.8
18	1	0.2	0.100%	0–8	0.5–2	2	28	20	2	94.5	10.3
19	1	0.2	0.500%	0–8	0.5–2	2	28	20	2	134.8	13.4
20	1	0.2	0.800%	0–8	0.5–2	2	28	20	2	82.9	9.7
21	1	0.2	0.100%	0–8	10–30	3	28	20	2	122.6	9.1
22	1	0.2	0.500%	0–8	10–30	3	28	20	2	154.4	10.8
23	1	0.2	0.800%	0–8	10–30	3	28	20	2	120.4	11.0
24	1	0.2	0.100%	0–8	10–30	2	28	20	2	129.1	13.0
25	1	0.2	0.500%	0–8	10–30	2	28	20	2	139.1	11.7
26	1	0.2	0.800%	0–8	10–30	2	28	20	2	141.5	13.4
27	1	0.33	0.000%	40–80	5–15	1	28	20	3	84.8	4.0
28	1	0.33	0.025%	40–80	5–15	1	28	20	3	90.1	4.3
29	1	0.33	0.050%	40–80	5–15	1	28	20	3	95.6	4.6
30	1	0.33	0.100%	40–80	5–15	1	28	20	3	97.2	5.2
31	1	0.35	0.000%	20–40	5–15	1	28	25	4	77.4	11.0
32	1	0.35	0.050%	20–40	5–15	1	28	25	4	82.9	11.7
33	1	0.35	0.080%	20–40	5–15	1	28	25	4	83.1	15.8
34	1	0.35	0.100%	20–40	5–15	1	28	25	4	84.5	15.0
35	1	0.35	0.120%	20–40	5–15	1	28	25	4	80.8	13.1
36	1	0.35	0.150%	20–40	5–15	1	28	25	4	73.0	10.5
37	1	0.4	0.500%	10–30	0.5–500	5	28	30	5	69.4	9.6
38	1	0.4	0.500%	10–30	0.5–500	1	28	30	5	72.1	10.0
39	1	0.4	0.030%	10–20	10–30	1	3	25	2	43.1	8.7
40	1	0.4	0.030%	20–30	10–30	1	3	25	2	40.1	7.7
41	1	0.4	0.030%	30–50	10–30	1	3	25	2	39.6	7.6
42	1	0.4	0.030%	10–20	10–30	1	7	25	2	56.7	9.8
43	1	0.4	0.030%	20–30	10–30	1	7	25	2	56.0	8.6
44	1	0.4	0.030%	30–50	10–30	1	7	25	2	53.2	9.2
45	1	0.4	0.030%	10–20	10–30	1	28	25	2	72.2	12.7
46	1	0.4	0.030%	20–30	10–30	1	28	25	2	73.6	11.5
47	1	0.4	0.030%	30–50	10–30	1	28	25	2	68.6	9.8
48	1	0.4	0.080%	10–20	10–30	1	3	25	2	43.8	6.3
49	1	0.4	0.080%	20–30	10–30	1	3	25	2	42.4	7.1
50	1	0.4	0.080%	30–50	10–30	1	3	25	2	39.4	6.9
51	1	0.4	0.080%	10–20	10–30	1	7	25	2	52.5	8.5
52	1	0.4	0.080%	20–30	10–30	1	7	25	2	52.5	8.4
53	1	0.4	0.080%	30–50	10–30	1	7	25	2	43.6	8.3
54	1	0.4	0.080%	10–20	10–30	1	28	25	2	65.6	11.8
55	1	0.4	0.080%	20–30	10–30	1	28	25	2	64.9	10.5
56	1	0.4	0.080%	30–50	10–30	1	28	25	2	63.5	10.7
57	1	0.4	0.150%	10–20	10–30	1	3	25	2	35.2	7.4
58	1	0.4	0.150%	20–30	10–30	1	3	25	2	43.2	7.4
59	1	0.4	0.150%	30–50	10–30	1	3	25	2	35.7	9.0
60	1	0.4	0.150%	10–20	10–30	1	7	25	2	63.9	11.0
61	1	0.4	0.150%	20–30	10–30	1	7	25	2	56.9	9.4
62	1	0.4	0.150%	30–50	10–30	1	7	25	2	58.3	10.4
63	1	0.4	0.150%	10–20	10–30	1	28	25	2	82.2	13.2
64	1	0.4	0.150%	20–30	10–30	1	28	25	2	78.0	11.4
65	1	0.4	0.150%	30–50	10–30	1	28	25	2	81.0	12.0
66	1	0.4	0.250%	10–20	10–30	1	3	25	2	44.0	7.4
67	1	0.4	0.250%	20–30	10–30	1	3	25	2	40.7	7.4
68	1	0.4	0.250%	30–50	10–30	1	3	25	2	41.2	8.8
69	1	0.4	0.250%	10–20	10–30	1	7	25	2	62.4	11.0

(*continued on next page*)

Table A1 (*continued*)

Input										Output	
No	Composites composition			Properties of CNTs			Treatment conditions			Mechanical properties	
	Type of cement	w/c	Content of CNTs	External diameter (nm)	Length (μm)	Functionalization method	Curing days	Curing temperature (℃)	Dispersion method	CS (MPa)	FS (MPa)
70	1	0.4	0.250%	20–30	10–30	1	7	25	2	59.4	9.4
71	1	0.4	0.250%	30–50	10–30	1	7	25	2	57.3	10.4
72	1	0.4	0.250%	10–20	10–30	1	28	25	2	84.1	13.2
73	1	0.4	0.250%	20–30	10–30	1	28	25	2	82.5	11.7
74	1	0.4	0.250%	30–50	10–30	1	28	25	2	82.0	12.0
75	1	0.4	0.030%	10–30	0.5–2	1	3	25	2	42.0	7.7
76	1	0.4	0.080%	10–30	0.5–2	1	3	25	2	39.5	7.0
77	1	0.4	0.150%	10–30	0.5–2	1	3	25	2	40.4	8.6
78	1	0.4	0.250%	10–30	0.5–2	1	3	25	2	42.1	9.9
79	1	0.4	0.030%	10–30	0.5–2	1	7	25	2	58.7	10.1
80	1	0.4	0.080%	10–30	0.5–2	1	7	25	2	51.4	7.7
81	1	0.4	0.150%	10–30	0.5–2	1	7	25	2	58.0	10.5
82	1	0.4	0.250%	10–30	0.5–2	1	7	25	2	64.0	11.8
83	1	0.4	0.030%	10–30	0.5–2	1	28	25	2	74.7	12.1
84	1	0.4	0.080%	10–30	0.5–2	1	28	25	2	64.3	10.1
85	1	0.4	0.150%	10–30	0.5–2	1	28	25	2	74.9	12.8
86	1	0.4	0.250%	10–30	0.5–2	1	28	25	2	81.8	14.8
87	2	0.5	0.000%	4–13	>1	1	7	20	1	36.9	7.6
88	2	0.5	0.050%	4–13	>1	1	7	20	1	35.1	6.5
89	2	0.5	0.100%	4–13	>1	1	7	20	1	32.0	6.0
90	2	0.5	0.250%	4–13	>1	1	7	20	1	35.4	5.7
91	2	0.5	0.500%	4–13	>1	1	7	20	1	27.3	6.7
92	2	0.5	0.000%	4–13	>1	1	28	20	1	49.7	7.8
93	2	0.5	0.050%	4–13	>1	1	28	20	1	57.3	7.9
94	2	0.5	0.100%	4–13	>1	1	28	20	1	52.3	7.5
95	2	0.5	0.250%	4–13	>1	1	28	20	1	54.0	7.4
96	2	0.5	0.500%	4–13	>1	1	28	20	1	52.0	7.5
97	1	0.45	0.000%	10–20	10–30	1	28	23	5	53.9	11.6
98	1	0.45	0.044%	10–20	10–30	1	28	23	5	56.2	11.6
99	1	0.45	0.088%	10–20	10–30	1	28	23	5	54.9	11.4
100	1	0.45	0.100%	10–20	10–30	1	28	23	5	58.2	11.0
101	1	0.45	0.200%	10–20	10–30	1	28	23	5	54.9	12.0
102	1	0.45	0.300%	10–20	10–30	1	28	23	5	56.2	12.5
103	1	0.45	0.044%	10–20	10–30	2	28	23	5	55.3	10.7
104	1	0.45	0.088%	10–20	10–30	2	28	23	5	55.3	10.9
105	1	0.45	0.100%	10–20	10–30	2	28	23	5	55.6	11.2
106	1	0.45	0.200%	10–20	10–30	2	28	23	5	54.3	12.3
107	1	0.45	0.300%	10–20	10–30	2	28	23	5	49.7	12.4
108	1	0.4	0.000%	10–20	10–30	1	28	23	2	74.9	10.5
109	1	0.4	0.030%	10–20	10–30	1	28	23	2	82.2	11.1
110	1	0.4	0.080%	10–20	10–30	1	28	23	2	80.0	10.7
111	1	0.4	0.150%	10–20	10–30	1	28	23	2	86.0	13.5
112	1	0.4	0.250%	10–20	10–30	1	28	23	2	91.4	16.3
113	1	0.4	0.350%	10–20	10–30	1	28	23	2	89.8	16.4
114	1	0.4	0.500%	10–20	10–30	1	28	23	2	94.3	16.9

Declaration of competing interest

The authors declare that they have no known competing financial interests or personal relationships that could have appeared to influence the work reported in this paper.

Acknowledgments

The authors acknowledge the supports provided by the National Natural Science Foundation of China (Grant No. 11872245) and the Research Grants Council of the Hong Kong Special Administrative Region, China (Project No. 9042644, CityU 11205518).

References

[1] Shi T, Li Z, Guo J, Gong H, Gu C. Research progress on CNTs/CNFs-modified cement-based composites – A review. Constr Build Mater 2019;202:290–307.
[2] Konsta-Gdoutos MS, Metaxa ZS, Shah SP. Multi-scale mechanical and fracture characteristics and early-age strain capacity of high performance carbon nanotube/cement nanocomposites. Cem Concr Compos 2010;32(2):110–5.
[3] Constantinides G. Nanoscience And Nanoengineering Of Cement-Based Materials. Woodhead Publishing; 2013.
[4] Chen ZS, Zhou X, Wang X, Guo P. Mechanical behavior of multilayer GO carbon-fiber cement composites. Constr Build Mater 2018;159:205–12.
[5] Liebscher M, Curosu I, Mechtcherine V, Drechsler A, Michel S. High-strength, strain-hardening cement-based composites (HS-SHCC) made with different high-performance polymer fibers. In: International Congress on Polymers in Concrete, 2018. p. 375-381, Springer.
[6] Tuncel EY, Pekmezci BY. Performance of glass fiber-reinforced cement composites containing phase change materials. Environ Prog Sustain 2019;38(3):e13061. https://doi.org/10.1002/ep.v38.310.1002/ep.13061.
[7] Song HQ, Zheng TL. Mechanical properties of steel fibre-reinforced high strength concrete with high early-age strength used in freezing shaft lining. In: Applied Mechanics and Materials, 2012. p. 1388-1393, Trans Tech Publications Ltd.
[8] Liew KM, Kai MF, Zhang LW. Carbon nanotube reinforced cementitious composites: An overview. Compos Part A Appl Sci Manuf 2016;91:301–23.
[9] Sindu BS, Sasmal S. Properties of carbon nanotube reinforced cement composite synthesized using different types of surfactants. Constr Build Mater 2017;155:389–99.
[10] Hu Y, Liew K, Wang Q, He X, Yakobson B. Nonlocal shell model for elastic wave propagation in single- and double-walled carbon nanotubes. J Mech Phys Solids 2008;56(12):3475–85.
[11] Liew KM, Kai MF, Zhang LW. Mechanical and damping properties of CNT-reinforced cementitious composites. Compos Struct 2017;160:81–8.

[12] Kumar S, Kolay P, Malla S, Mishra S. Effect of multiwalled carbon nanotubes on mechanical strength of cement paste. J Mater Civil Eng 2012;24(1):84–91.
[13] Luo JL, Duan ZD, Zhao TJ, Li QY. Effect of multi-wall carbon nanotube on fracture mechanical property of cement-based composite. In: Advanced Materials Research, 2010. p. 581-584, Trans Tech Publications Ltd.
[14] Sedaghatdoost A, Behfarnia K. Mechanical properties of Portland cement mortar containing multi-walled carbon nanotubes at elevated temperatures. Constr Build Mater 2018;176:482–9.
[15] Mohsen MO, Taha R, Abu Taqa A, Al-Nuaimi N, Al-Rub RA, Bani-Hani KA. Effect of nanotube geometry on the strength and dispersion of cnt-cement composites. J Nanomater 2017;2017:1–15.
[16] Abu Al-Rub RK, Ashour AI, Tyson BM. On the aspect ratio effect of multi-walled carbon nanotube reinforcements on the mechanical properties of cementitious nanocomposites. Constr Build Mater 2012;35:647–55.
[17] Li GY, Wang PM, Zhao X. Mechanical behavior and microstructure of cement composites incorporating surface-treated multi-walled carbon nanotubes. Carbon 2005;43(6):1239–45.
[18] Li GY, Wang PM, Zhao X. Pressure-sensitive properties and microstructure of carbon nanotube reinforced cement composites. Cem Concr Compos 2007;29 (5):377–82.
[19] Chan LY, Andrawes B. Finite element analysis of carbon nanotube/cement composite with degraded bond strength. Comp Mater Sci 2010;47(4).
[20] Singh AP, Gupta BK, Mishra M, Govind, Chandra A, Mathur RB, et al. Multiwalled carbon nanotube/cement composites with exceptional electromagnetic interference shielding properties. Carbon 2013;56:86–96.
[21] Ubertini F, Materazzi AL, D'Alessandro A, Laflamme S. Natural frequencies identification of a reinforced concrete beam using carbon nanotube cement-based sensors. Eng Struct 2014;60:265–75.
[22] Sobolkina A, Mechtcherine V, Khavrus V, Maier D, Mende M, Ritschel M, et al. Dispersion of carbon nanotubes and its influence on the mechanical properties of the cement matrix. Cem Concr Compos 2012;34(10):1104–13.
[23] Hassan NM, Fattah KP, Tamimi AK. Modelling mechanical behavior of cementitious material incorporating CNTs using design of experiments. Constr Build Mater 2017;154:763–70.
[24] Ramezani M, Kim YH, Sun Z. Modeling the mechanical properties of cementitious materials containing CNTs. Cem Concr Compos 2019;104:103347. https://doi.org/10.1016/j.cemconcomp.2019.103347.
[25] Rao HS, Mukherjee A. Artificial neural networks for predicting the macromechanical behaviour of ceramic-matrix composites. Comp Mater Sci 1996;5(4):307–22.
[26] Reddy TCS. Predicting the strength properties of slurry infiltrated fibrous concrete using artificial neural network. Front Struct Civ Eng 2018;12(4):490–503.
[27] Ji G, Li F, Li Q, Li H, Li Z. Prediction of the hot deformation behavior for Aermet100 steel using an artificial neural network. Comp Mater Sci 2010;48 (3):626–32.
[28] Ahmadi M, Naderpour H, Kheyroddin A. ANN model for predicting the compressive strength of circular steel-confined concrete. Int J Civ Eng 2017;15 (2):213–21.
[29] Yuvaraj P, Ramachandra Murthy A, Iyer NR, Sekar SK, Samui P. Support vector regression based models to predict fracture characteristics of high strength and ultra high strength concrete beams. Eng Fract Mech 2013;98:29–43.
[30] Yan K, Shi C. Prediction of elastic modulus of normal and high strength concrete by support vector machine. Constr Build Mater 2010;24(8):1479–85.
[31] Tinoco J, Gomes Correia A, Cortez P. Support vector machines applied to uniaxial compressive strength prediction of jet grouting columns. Comput Geotech 2014;55:132–40.
[32] Huang J, Liew J, Ademiloye A, Liew K. Artificial intelligence in materials modeling and design. Arch Computat Methods Eng 2020:1–15.
[33] Yu X. Support vector machine-based QSPR for the prediction of glass transition temperatures of polymers. Fiber Polym 2010;11(5):757–66.
[34] Gupta T, Sachdeva SN. Laboratory investigation and modeling of concrete pavements containing AOD steel slag. Cem Concr Res 2019;124:105808. https://doi.org/10.1016/j.cemconres.2019.105808.
[35] Lee S, Ha J, Zokhirova M, Moon H, Lee J. Background information of deep learning for structural engineering. Arch Computat Methods Eng 2018;25(1):121–9.
[36] Pei K, Cao Y, Yang J, Deepxplore JS. Automated whitebox testing of deep learning systems. In: In: Proceedings of the 26th Symposium on Operating Systems Principles. p. 1–18.
[37] Cui X, Han B, Zheng Q, Yu X, Dong S, Zhang L, et al. Mechanical properties and reinforcing mechanisms of cementitious composites with different types of multiwalled carbon nanotubes. Compos Part A Appl Sci Manuf 2017;103:131–47.
[38] Xu S, Liu J, Li Q. Mechanical properties and microstructure of multi-walled carbon nanotube-reinforced cement paste. Constr Build Mater 2015;76:16–23.
[39] Wang B, Han Yu, Pan B, Zhang T. Mechanical and morphological properties of highly dispersed carbon nanotubes reinforced cement based materials. J Wuhan Univ Technol 2013;28(1):82–7.
[40] del Carmen CM, Galao O, Baeza FJ, Zornoza E, Garcés P. Mechanical properties and durability of CNT cement composites. Materials 2014;7(3):1640–51.
[41] Torabian Isfahani F, Li W, Redaelli E. Dispersion of multi-walled carbon nanotubes and its effects on the properties of cement composites. Cem Concr Compos 2016;74:154–63.
[42] Mohsen MO, Taha R, Abu Taqa A, Shaat A. Optimum carbon nanotubes' content for improving flexural and compressive strength of cement paste. Constr Build Mater 2017;150:395–403.